Magnetic Resonance in Medicine 60:457–461 (2008)

MRI Thermometry: Fast Mapping of RF-Induced Heating Along Conductive Wires

Philipp Ehses,[1*] Florian Fidler,[2] Peter Nordbeck,[1,3] Eberhard D. Pracht,[1] Marcus Warmuth,[1] Peter M. Jakob,[1,2] and Wolfgang R. Bauer[3]

Conductive implants are in most cases a strict contraindication for MRI examinations, as RF pulses applied during the MRI measurement can lead to severe heating of the surrounding tissue. Understanding and mapping of these heating effects is therefore crucial for determining the circumstances under which patient examinations are safe. The use of fluoroptic probes is the standard procedure for monitoring these heating effects. However, the observed temperature increase is highly dependent on the positioning of such a probe, as it can only determine the temperature locally. Temperature mapping with MRI after RF heating can be used, but cooling effects during imaging lead to a significant underestimation of the heating effect. In this work, an MRI thermometry method was combined with an MRI heating sequence, allowing for temperature mapping *during* RF heating. This technique may provide new opportunities for implant safety investigations. Magn Reson Med 60:457–461, 2008. © 2008 Wiley-Liss, Inc.

Key words: thermometry; temperature mapping; proton resonance frequency; RF heating; MRI

With the growing number of MRI examinations in patients with metallic implants and the development of interventional MRI, monitoring of RF-induced heating of biological tissue adjacent to conductors has become increasingly important. Measuring these heating effects during an MRI examination is currently only possible in vitro or in an animal model with a temperature probe. Fluoroptic probes are most commonly used (1), although thermocouple wires can also be employed (2). A major drawback to these methods is that these probes can only measure the temperature at a single point, making it difficult or at least time-consuming to investigate heating effects of implants with complex geometries. It has been shown that positioning errors of fluoroptic probes may lead to an error of up to 45%, even if the probe is directly attached to the heating source (3). An alternative to this approach is to use MRI for the measurement of temperature changes. There are several MRI thermometry methods that have been proposed for such a measurement (4). In a prior study, one of these techniques was used to determine the temperature increase induced by a separate MRI sequence (5). However, this approach has a number of constraints; it does not monitor temperature dynamics, and heat dissipation following the interruption of the heating MRI sequence leads to an underestimation of the temperature increase. Another method is the use of an external RF transmitter for heating the wire/implant while monitoring the temperature increase with a standard MRI thermometry sequence (6). However, this approach does not monitor the heating effect of an MRI sequence or the MRI system but of the external RF transmitter. In this work, a new approach for MRI thermometry is presented that allows the determination of a temperature increase during RF heating caused by the MRI sequence *itself*. To this end, a proton resonance frequency (PRF) shift MRI thermometry method (7) was combined with an MRI heating sequence, which yielded a map of temperature changes induced by the heating part of the sequence. The results were validated with a fluoroptic temperature probe.

MATERIALS AND METHODS

General Setup

All experiments were performed on a 1.5T whole-body imaging system (Magnetom Vision; Siemens Medical Solutions, Erlangen, Germany) with a gradient field strength of 25 mT/m and a maximum slew rate of 83 mT/m/ms. Maximum output power of the RF tube was 15 kW. For signal detection, a four-channel phased-array surface coil was used.

The $350 \times 450 \times 160$ mm^3 polyvinyl chloride phantom was filled with 20 liter hydroxyethyl-cellulose (HEC) gel (Sigma Aldrich, Steinheim, Germany). A 5% concentration of the HEC gelling agent was chosen to minimize convection effects. The gel was doped with $CuSO_4$ (5 mmol/liter) to reduce the T_1 relaxation time to approximately 220 ms, in order to increase the signal-to-noise ratio (SNR) for short repetition times. Additionally, 1.0 g/liter cooking salt (NaCl) was added to reach the desired conductivity of 0.47 S/m, which has been proposed as a reasonable value for MRI heating experiments to match organic tissue (8).

Determination of the Proton Resonance Frequency Change Coefficient α

To determine the proton resonance frequency (PRF) change coefficient, a 50-ml syringe filled with the doped HEC gel was heated to 50°C. A fluoroptic probe was placed inside the 20-liter gel phantom. The temperature of the gel inside the phantom was approximately 18°C. The heated gel was then injected at the location of the fluoroptic

[1]Physikalisches Institut (EP 5), Universität Würzburg, Würzburg, Germany.
[2]Forschungszentrum Magnet-Resonanz-Bayern (MRB) e.V., Würzburg, Germany.
[3]Medizinische Klinik und Poliklinik I, Universität Würzburg, Würzburg, Germany.

Grant sponsor: Bayerische Forschungsstiftung (Bavarian Research Foundation), project "Entwicklung MR-kompatibler Schrittmacherelektroden."

*Correspondence to: Philipp Ehses, Experimentelle Physik 5, Universität Würzburg, Am Hubland, D-97074 Würzburg, Germany. E-mail: ehses@physik.uni-wuerzburg.de

Received 13 February 2007; revised 20 August 2007; accepted 23 August 2007.
DOI 10.1002/mrm.21417
Published online in Wiley InterScience (www.interscience.wiley.com).

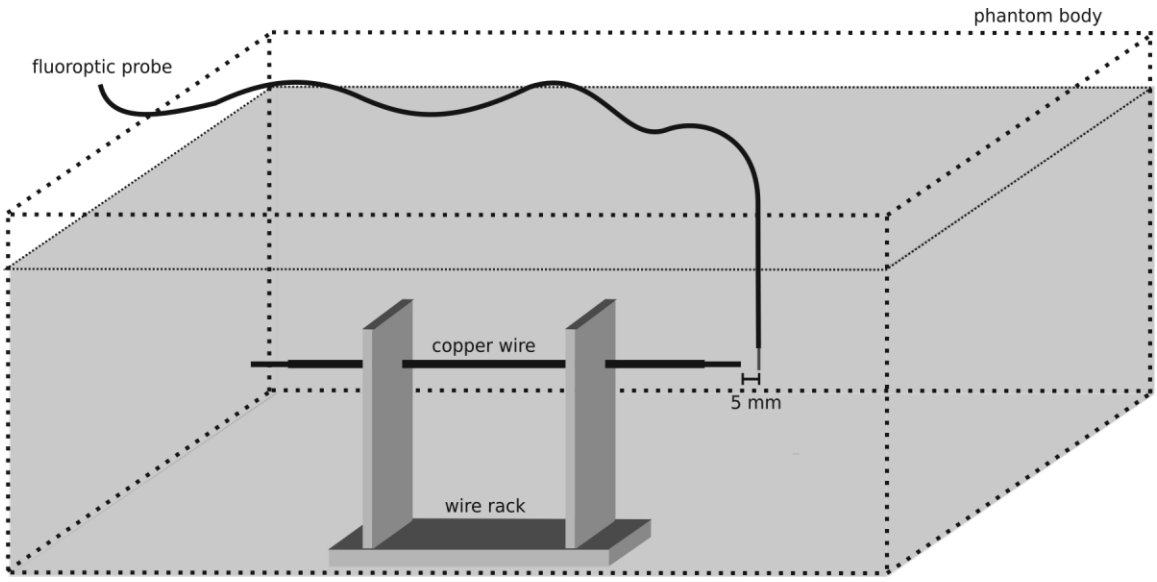

FIG. 1. Experimental setup.

probe, thereby forming a bubble of heated gel around the probe, during a continuous run of a gradient-recalled echo (GRE) sequence with the following parameters: repetition time (TR) = 50 ms, echo time (TE) = 15 ms, acquisition time (TA) = 6 s, flip angle (FA) = 50°, field-of-view in read direction (FOV) = 350 mm, slice thickness = 10 mm, slice orientation: transversal, bandwidth (BW) = 390 Hz/pixel, acquisition matrix size = 128 × 48 (3/8 rectangular FOV).

Thermometry of an RF-Heated Conductive Wire

A schematic representation of the experimental setup of the actual thermometry experiment is shown in Fig. 1. Specifically, a conductive wire was positioned at the middle left side of the phantom (40 mm from the left wall). The wire had a diameter of 1.2 mm and a length of 200 mm. The inner 180 mm were insulated by a silicone tube. To avoid susceptibility artifacts, a material with a susceptibility value close to that of water was selected. In the results shown here, a copper wire was employed. The magnetic susceptibility of copper is close to that of water (-9.63×10^{-6} and -9.05×10^{-6} (9), respectively) so that almost no susceptibility artifacts should be expected.

For validation purposes, a fluoroptic thermometry system was used (Model m3300; Luxtron, Santa Clara, CA, USA) as recommended by the American Society for Testing and Materials (ASTM) International standard for measurement of RF-induced heating near passive implants during MRI (10). According to the manufacturer, the fluoroptic probe has an accuracy of 0.5°C within 50°C of the calibration point and a response time of 0.25 s. The probe was attached to the wire such that the end of the probe was 5 mm beyond the tip of the wire (head side of the phantom).

Temperature mapping was performed using a modified PRF shift method (7), containing an off-resonant high-power RF pulse (sinc profile) that served to heat the phantom filling. The imaging sequence was based on an RF-spoiled GRE sequence. After the slice refocusing gradient, an off-resonant heating pulse was inserted to allow for the adjustment of the specific absorption rate by variation of the FA. To assure that the additional RF pulse did not influence imaging, its frequency was chosen to be 128 kHz (0.2%) smaller than the PRF (PRF = 63.86 MHz). A graphical representation of the pulse sequence is given in Fig. 2.

A total of 100 phase-contrast images were acquired in the sagittal orientation consecutively. The slice was positioned directly through the wire. The sequence parameters were as follows: TR = 30 ms, TE = 20 ms, TA = 3.9 s, FA = 30°, FOV = 400 mm, slice thickness = 5 mm, BW = 390 Hz/pixel, acquisition matrix size = 96 × 256 (3/8 rectangular FOV). The averaged RF power of the experiment was set to 9 W/kg bodyweight by adjusting the power of the heating pulse via its FA while observing the system's specific absorption rate (SAR) monitor. This resulted in a FA of 520°. The duration of the additional RF pulse was set to 2 ms to reduce RF tube load.

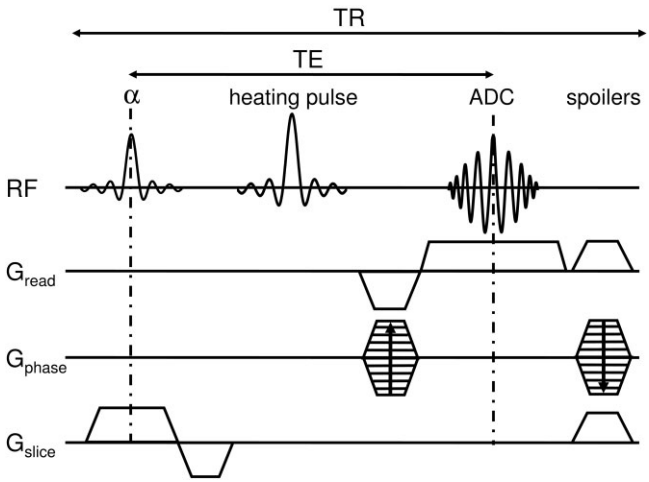

FIG. 2. GRE sequence including an off-resonant heating pulse as used in the thermometry experiments.

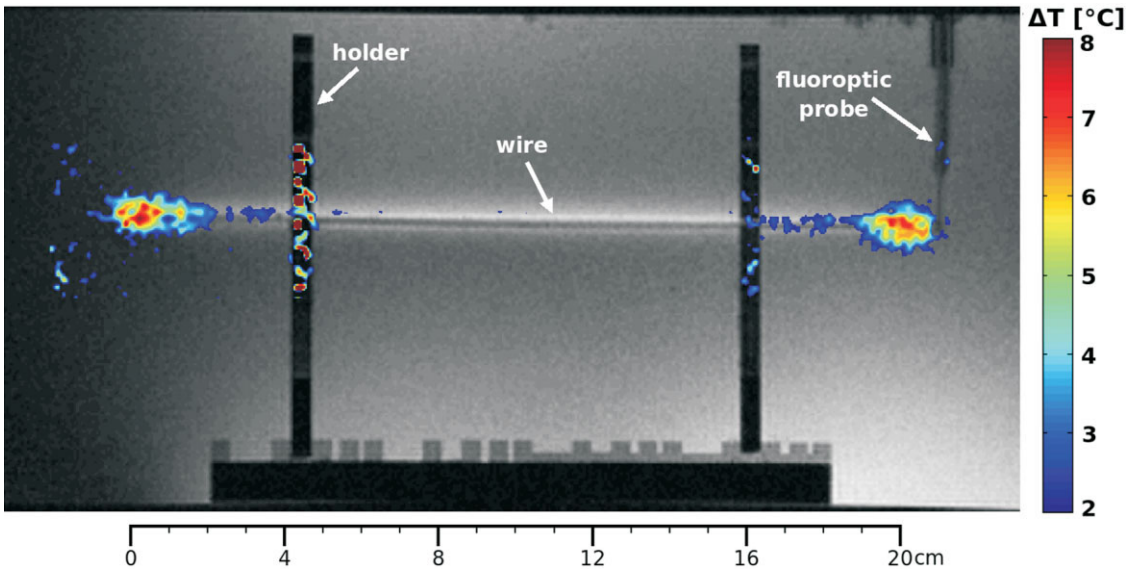

FIG. 3. Overlay of a scout image and the PRF shift temperature map after the 7-min heating period. Both images were interpolated to a matrix size of 384 × 1024 (two-fold interpolation of the scout and four-fold interpolation of the temperature map). Only temperature differences larger than 2°C and in an area 20 mm adjacent to the wire are shown. Pronounced hot spots are visible at both tips of the wire.

The temperature rise was obtained by subtracting each phase-contrast image from a reference image, which yielded the change of the image phase $\Delta\Phi$ in every pixel. To simplify the measurement protocol, the first acquired phase contrast image served as the reference image, so that a total of 99 temperature maps were obtained. It is important to note that there is a slight underestimation of the temperature increase because the temperature had already begun to increase during the acquisition of this reference. The temperature changes ΔT were then obtained by using the following equation (4,7)

$$\Delta T = \frac{\Delta\phi}{\alpha\gamma B_0 TE}, \qquad [1]$$

where γ is the gyromagnetic ratio for protons ($\gamma/2\pi$ = 42.57 MHz/T) and B_0 represents the strength of the main magnetic field. The temperature dependency of the PRF is given by the PRF change coefficient α, which is approximately −0.01 ppm/°C for water and aqueous tissue.

RESULTS

The PRF change coefficient was calculated by subtracting the image phases before the injection of the heated gel from those acquired after the injection, averaged over the center of the "heat bubble" where the temperature distribution was expected to be uniform. The fluoroptic probe was used as a reference and provided the temperature difference after injection. Rearranging Eq. [1], the PRF change coefficient α was determined to be 0.00971 ppm/°C with a mean SD of 0.00081 ppm/°C. This is in agreement with values from previous publications (7,11).

An overlay of the temperature map at the end of the 7 min heating interval and a scout image (GRE-sequence) is shown in Fig. 3. The heating effect of the wire can be clearly seen by the spreading of the heat into the surrounding gel at both wire tips. Figure 4 shows the temperature of the gel 5 mm beyond the wire tip as measured by the fluoroptic probe in comparison to the results of the MRI temperature measurements averaged over a region of interest. The region of interest consisted of two pixels approximately 4 mm beyond the tip of the wire. The exact position of the fluoroptic probe had to be excluded in the region of interest as the probe led to significant signal losses at its location due to partial volume effects. The total size of the chosen region of interest was 5.0 × 1.56 × 3.13 mm^3 (x, y, z axis of the scanner) compared to the diameter of the sensor of 1 mm and its sensitive length of 4 mm in the y-direction. Despite these differences in orientation and size of their respective sensitive regions, the measurements from the fluoroptic probe and MRI thermometry led to qualitatively comparable results.

The averaged MRI temperature values were fit to the following simple temperature model:

$$T(t) = T(0) + (T(\infty) - T(0)) \cdot (1 - e^{-kt}), \qquad [2]$$

where the baseline temperature is given as T(0) = 0 and the theoretical temperature in an infinitely large phantom after an infinite period of heating is T(∞).The χ^2 value of the fit was 0.40 (°C)^2. The temperature increase during the acquisition of the first phase-contrast image (reference) was estimated from this fit to be approximately 0.3°C (in the chosen region of interest). To adjust for the slight underestimation of the temperature increase, this value was added to the MRI measured temperature in the graph of Fig. 4.

DISCUSSION AND CONCLUSIONS

This work shows that MRI heating and MRI temperature mapping can be combined to form a powerful tool that

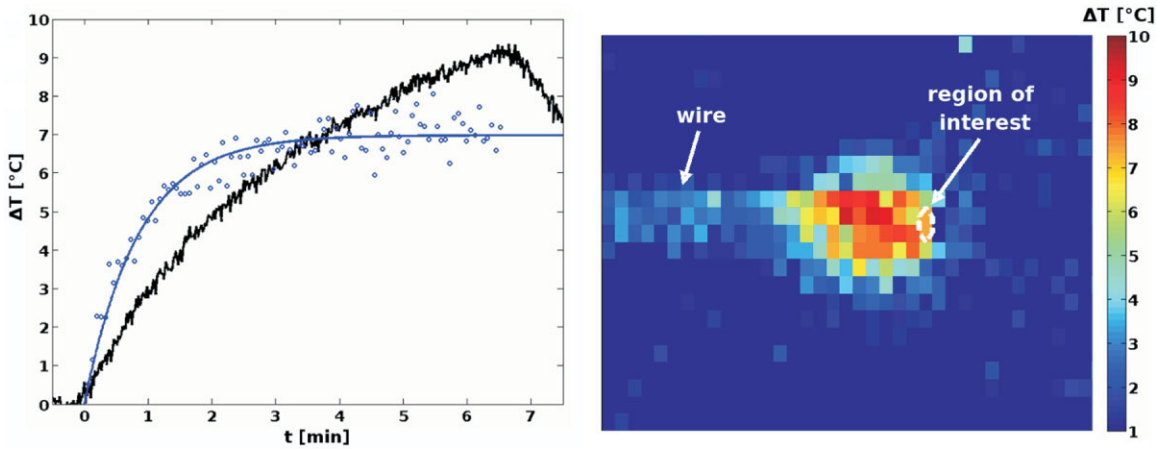

FIG. 4. Left: Temperature from the MRI temperature maps averaged over a two-pixel region of interest (blue line) in comparison to the readings from the fluoroptic probe (black line). The MRI measured temperature distribution near the wire tip is depicted on the right. The temperature was averaged over the two pixels in the region indicated by the white dotted line (approximately 4 mm beyond the tip of the wire).

overcomes the disadvantage of a single point temperature measurement by a fluoroptic probe. The accuracy achieved in this study was sufficient for observing the temperature increase qualitatively. Further work will have to be done in order to achieve a measurement precision comparable to fluoroptic probe thermometry.

Comparing the readings from the fluoroptic probe with the MRI measured temperature increase, it is perceivable that the MRI measurement reaches equilibrium earlier and has a smaller maximum value. The former is easily explainable as the chosen region of interest is closer to the tip of the wire, so that inertia is expected to be smaller. However, there is no simple explanation for the smaller maximum value of the MRI measured temperature as one would expect just the opposite. It is possible though, that there were systematic errors in the determination of the PRF change coefficient α. Additionally, eddy currents may have caused imaging artifacts in the immediate vicinity of the wire. As the intention of the shown experiments was to identify possible hot spots rather than to accurately quantify the temperature rise, this effect was not investigated in detail.

To estimate the error due to imaging noise in the modified MRI thermometry method, a map of the local mean SDs was calculated from the set of acquired phase-contrast images (Fig. 5). As expected, the mean SD is high in areas where heating occurred, as the image phase changed over time. Outside these heating areas, the mean SD is much smaller and depends on the position and geometry of the receiver coil. The coil position was optimized for high SNR at one wire tip, so that the noise at the other tip was much higher. The mean SD caused by image noise in the chosen region of interest was extrapolated from the surrounding to be approximately 0.5°C. The associated error is too small to explain the discrepancy mentioned in the previous paragraph.

There are several more reasons why a quantitative comparison of the measurements from the probe and MRI is complex. The degree of agreement is highly dependent on the choice of the region of interest over which the mea-

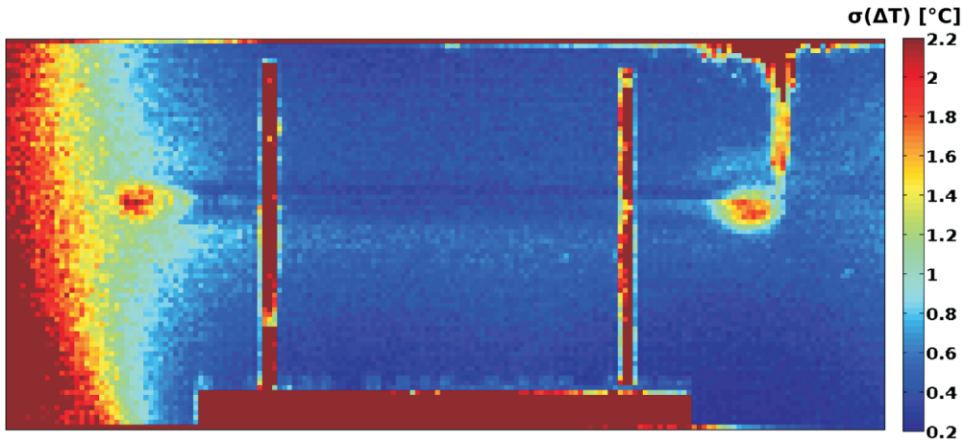

FIG. 5. Map of mean SD, calculated from the set of phase-contrast images for every pixel separately, and translated into temperature values.

sured temperature is averaged and on the positioning of the fluoroptic probe. In addition, it is impossible to obtain an MRI signal from the exact location of the fluoroptic probe at all. Therefore, an unflawed quantitative comparison is not viable.

Additionally, it is possible that the probe may interfere with the local temperature increase as an additional artificial structure is put directly into the region in question. The value of the probe in temperature measurement is diminished if it changes the system to be observed significantly and unpredictably. Conversely, the effect of MRI thermometry on the implant heating can be easily quantified. It depends solely on the power contribution of the MRI thermometry module in the imaging sequence. Since this contribution is two orders of magnitude smaller than that of the heating pulse, it can be neglected.

This highlights the main advantages and disadvantages of these two methods: MRI thermometry in the immediate vicinity of the wire (or other implants) is difficult to perform. However, even though a fluoroptic probe might in general be sensible to achieve very accurate measurement results, the temperature readings are highly dependent on its position. Even small displacements of the sensor can strongly influence the measured temperature values, especially in close vicinity to a hot spot (3). Good reproducibility is therefore hard to achieve. The dependency of MRI thermometry on slice positioning is not so problematic, as the temperature measured originates from a relatively large voxel and the region of interest can be chosen retrospectively (e.g., with the help of a high-resolution magnitude image). Furthermore, possible hot spots along large implants with a complex shape can be easily identified in one MRI temperature measurement.

Therefore, the combination of MRI thermometry and the use of a temperature sensor may be very beneficial in MRI safety investigations. A sensible course of action may be to identify occurring hot spots in a preliminary experiment using MRI thermometry. The most prominent spots can then be further investigated in a second experiment using a suitable temperature probe.

The method of using an RF pulse that does not influence the spin system for heating can be combined with any MRI temperature mapping technique, or more generally, with any MRI sequence. Changing the frequency of the heating pulse by a few tenths of a percent renders MRI thermometry possible without changing its heating capabilities. An improved version, which is less motion sensitive, such as one that is based on referenceless PRF shift thermometry (12) or using an appropriate T_1-based sequence, may have the potential for in vivo and noninvasive temperature monitoring of an MRI examination in an animal model.

However, a major drawback of the proposed technique is that MRI thermometry on most standard implants is hardly possible due to severe susceptibility artifacts. It is then necessary to use specially fabricated implants that are susceptibility-matched to the surrounding material (water and organic tissue). Fortunately, there are appropriate materials available, such as copper or carbon, if biocompatibility is essential. Konings et al. (13) have already stated that heating capabilities mainly depend on the conductivity of the material and not on the type of material itself. Therefore, replacing the material of the original implant by one that is susceptibility-matched to organic tissue would hardly influence its heating capabilities.

The method presented here can be used in safety testing environments for the noninvasive monitoring of the heating of implants during MRI examinations.

REFERENCES

1. Armenean C, Perrin E, Armenean M, Beuf O, Pilleul F, Saint-Jalmes H. RF-induced temperature elevation along metallic wires in clinical magnetic resonance imaging: influence of diameter and length. Magn Reson Med 2004;52:1200–1206.
2. Luechinger R, Zeijlemaker VA, Pedersen EM, Mortensen P, Falk E, Duru F, Candinas R, Boesiger P. In vivo heating of pacemaker leads during magnetic resonance imaging. Eur Heart J 2005;26:376–383.
3. Mattei E, Triventi M, Calcagnini G, Censi F, Kainz W, Bassen HI, Bartolini P. Temperature and SAR measurement errors in the evaluation of metallic linear structures heating during MRI using fluoroptic probes. Phys Med Biol 2007;52:1633–1646.
4. Quesson B, de Zwart JA, Moonen CT. Magnetic resonance temperature imaging for guidance of thermotherapy. J Magn Reson Imaging 2000; 12:525–533.
5. Levine D, Zuo C, Faro CB, Chen Q. Potential heating effect in the gravid uterus during MR HASTE imaging. J Magn Reson Imaging 2001;13: 856–861.
6. Qiu B, El-Sharkawy AM, Paliwal V, Karmarkar P, Gao F, Atalar E, Yang X. Simultaneous radiofrequency (RF) heating and magnetic resonance (MR) thermal mapping using an intravascular MR imaging/RF heating system. Magn Reson Med 2005;54:226–230.
7. Ishihara Y, Calderon A, Watanabe H, Okamoto K, Suzuki Y, Kuroda K, Suzuki Y. A precise and fast temperature mapping using water proton chemical shift. Magn Reson Med 1995;34:814–823.
8. Kainz W. Draft: SAR intercomparison protocol for 1.5 T MR systems. U.S. Food and Drug Administration, Center for Devices and Radiological Health, Office of Science and Engineering Laboratories & Office of Device Evaluation; 2006.
9. Schenck JF. The role of magnetic susceptibility in magnetic resonance imaging: MRI magnetic compatibility of the first and second kinds. Med Phys 1996;23:815–850.
10. American Society for Testing and Materials (ASTM) International. F2182–02 test method for measurement of radio frequency induced heating near passive implants during magnetic resonance imaging. West Conshohocken, PA: American Society for Testing and Materials (ASTM) International; 2003.
11. MacFall JR, Prescott DM, Charles HC, Samulski TV. 1H MRI phase thermometry in vivo in canine brain, muscle, and tumor tissue. Med Phys 1996;23:1775–1782.
12. Rieke V, Vigen KK, Sommer G, Daniel BL, Pauly JM, Butts K. Referenceless PRF shift thermometry. Magn Reson Med 2004;51:1223–1231.
13. Konings MK, Bartels LW, Smits HF, Bakker CJ. Heating around intravascular guidewires by resonating RF waves. J Magn Reson Imaging 2000;12:79–85.